Electrocrystallization of Calcium Phosphates

Noam Eliaz
Biomaterials and Corrosion Laboratory, School of Mechanical Engineering and
The Materials Science and Engineering Program, Tel Aviv University, Tel Aviv 69978, Israel

(*Received 27 March 2008; accepted 10 July 2008*)

Abstract. The interest in electrocrystallization of calcium phosphates (CaP) in general, and of hydroxyapatite (HAp) specifically, results from the promising industrial benefits, unique microstructures, and properties of the deposits produced by this process, and the possible similarity to bone mineralization in vivo. In this paper, our work on electrocrystallization of HAp and octacalcium phosphate (OCP) on CP-Ti and Ti-6Al-4V alloy, in solution containing calcium nitrate and ammonium dihydrogen phosphate, is briefly reviewed. The early stages of nucleation and growth are characterized in real time by means such as electrochemical quartz crystal microbalance (EQCM) and electrochemical atomic force microscope (EC-AFM). The change in growth mode and the role of precursors to HAp are explained. The role of charge transfer and local increase in pH is discussed.

INTRODUCTION

Biocompatibility (i.e., the ability of a material to perform with an appropriate host response in a specific application) and corrosion resistance are two important factors in the selection of biomaterials. Corrosion control in vivo is currently limited mainly to careful design of the device, proper material selection, and surface modification.[1] New materials and customized medical devices can be produced by advanced processes such as three-dimensional printing.[2,3] Surface modification by electrochemical processes is gaining much interest. On the one hand, electrochemical polishing (electropolishing) can yield a smooth surface, free of contaminants and internal stresses, more passive, with an increased resistance against bacteria growth and a reduced protein adsorption, which are helpful in preventing ingrowth of tissue (e.g., restenosis in stent applications).[4] On the other hand, chemical deposition and electrochemical deposition can be used to form either monolayers or coatings of synthetic materials on devices, possibly while incorporating biological matter and drugs in the deposit, e.g., for enhancing the osseointegration of an orthopedic implant. This paper focuses on the latter.

Apatite is the primary inorganic constituent of all mammalian skeletal and dental tissues. It belongs to the family of calcium phosphates (CaP), which includes, among others, hydroxyapatite (HAp, $Ca_5(PO_4)_3(OH)$), α- and β-tricalcium phosphates (TCP, $Ca_3(PO_4)_2$), octacalcium phosphate (OCP, $Ca_4(HPO_4)(PO_4)_2{\cdot}2.5H_2O$), dibasic calcium phosphate dihydrate (brushite, DCPD, $CaHPO_4{\cdot}2H_2O$), dibasic calcium phosphate anhydrous (monetite, DCPA, $CaHPO_4$), and amorphous calcium phosphate (ACP, $Ca_3(PO_4)_2{\cdot}xH_2O$, x = 3–4.5).[5,6] Wet

E-mail: neliaz@eng.tau.ac.il

DOI 10.1560/IJC.48.3-4.159

cortical bone, for example, is composed of 69 wt% inorganic (mineral) constituent, 22 wt% organic matrix, and 9 wt% absorbed water. Biological apatites deviate from the stoichiometric composition of HAp, and contain small amounts of Mg^{2+}, Na^{+}, K^{+}, CO_3^{2-}, Cl^{-}, and F^{-}. They have an hexagonal crystallographic structure (not close-packed),[7] and grow as platelets with typical length, width, and thickness of 30–120 nm, 25–120 nm, and 1.5–9 nm, respectively.[8–11] In their synthetic form, apatites are typically bioactive ceramics (i.e., materials that elicit specific biological response at the interface), which are more osteoconductive than metal surfaces and form direct bonds with adjacent hard tissues[12] via dissolution and ion exchange with body fluids. Hence, several types of synthetic apatites are now commercially available for use in bone repair, bone augmentation, bone substitution, and as coatings on dental and orthopedic implants.

Several methods have been explored to deposit CaP coatings in order to enhance implant fixation. Plasma spraying is the most common technology used commercially. Since the early 1990s, however, much interest in electrodeposition has evolved due to: (1) the low temperatures involved, which enable formation of highly crystalline deposits with low solubility in body fluids and low residual stresses; (2) the ability to coat porous, geometrically complex, or non line-of-sight surfaces; (3) the ability to control the thickness, composition, and microstructure of the deposit; (4) the possible improvement of the substrate/coating bond strength; and (5) the availability and low cost of equipment.

Electrocrystallization (i.e., the nucleation and crystal growth in electrochemical systems under the influence of an electric field) can be treated in a manner similar to deposition from a vapor phase. The nucleation type can be either instantaneous or progressive, and the growth mode can be one-, two-, or three-dimensional, with the resulting shape of growing crystallites being, for example, needles, discs, and either cones or hemispheres, respectively. The rate-determining step may be charge transfer, cylindrical diffusion, hemispherical diffusion, or Ohmic polarization. Different combinations of nucleation type, growth mode, and rate-determining step yield different functions of current density as a function of time.[13]

In this paper, the work that has been carried out at Tel Aviv University is reviewed. The early stages of nucleation and growth are characterized.[14,15] The change in growth mode and the role of precursors to HAp are explained. The role of charge transfer and local increase in pH is discussed. The effects of bath pH and temperature are discussed briefly.[16,17] Other aspects, such as the structure, chemical composition and surface morphology of the coatings,[16–18] coating wettability,[19] its adhesion to the substrate,[20,21] its corrosion resistance,[16,18] and the biologic response as evaluated both in vitro[19,21] and in vivo[22,23] shall not be reviewed in this paper in detail. Yet, the main conclusions drawn in those papers are summarized in the following two paragraphs. In addition, electrophoretic deposition of HAp on 316L stainless steel[24,25] will not be discussed.

In our previous studies, the electrodeposition of uniform, single-phase, stoichiometric HAp coatings on CP-Ti was demonstrated.[18] The bath temperature was found to have an important effect on the ability to get good coatings, with an optimum reached somewhere between 70 and 95 °C.[17] The composition and pH of the bath were found to significantly affect the nature and surface morphology of the CaP coatings. Coatings deposited at $pH_0 = 4.2$ were thicker, less crystallized, and more porous than coatings deposited at $pH_0 = 6.0$, and also revealed traces of OCP (and, possibly, of DCPA). Samples coated at $pH_0 = 6.0$ also exhibited better corrosion resistance. The content of OCP in coatings deposited at pH = 4.2 was decreased as a result of increasing the bath temperature. Texture (preferred orientation) of HAp was observed, both at $pH_0 = 4.2$ and at $pH_0 = 6.0$. Similarity on the nanoscale was observed to the morphology of HAp crystals in mature human dental enamel. The addition of KCl to the bath resulted in the formation of Ca-enriched, thicker coatings, with a different surface morphology of needles. The addition of $NaNO_2$ also resulted in thicker coatings, but with a less pronounced preferred orientation and a dendritic surface morphology. Speciation–precipitation calculations were made in order to better understand the thermodynamic driving forces.[16] Cyclic potentiodynamic polarization scans in Ringer's solution revealed smaller hysteresis loops for HAp-coated samples compared to bare CP–Ti, thus indicating good resistance of the coated samples against localized corrosion.[18]

In vivo studies were carried out in two stages. First, three different rods, bare Ti–6Al–4V alloy, Ti–6Al–4V alloy coated with plasma-sprayed HAp (PS-HAp), and Ti–6Al–4V alloy coated with electrochemically deposited HAp (ED-HAp), were implanted in the USA into canine trabecular bone for 6 hours, 7 days, and 14 days. Environmental scanning electron microscopy (ESEM) study showed that PS-HAp coatings had higher bone apposition ratios than those exhibited by bare Ti–6Al–4V and ED-HAp coatings after 7 days. The PS-HAp was found to be of lower crystallinity and higher solubility compared to ED-HAp. At 14 days after implantation, ED-HAp and PS-HAp coatings exhibited similar bone apposition ratios, much higher than that for the uncoated alloy. In spite of poor adhesion of ED-HAp coatings to

the Ti–6Al–4V substrate, in the absence of proper surface preparation, the surface morphology and higher surface area of ED-HAp coatings apparently resulted in better mechanical integration between the coating and the mineralized tissue.[22] In the second stage, similar rod implants were activated chemically and then grit-blasted with high-purity alumina. Some of the implants were also treated chemically in 5 M NaOH solution at 60 °C. Three groups of samples were prepared at Tel Aviv University: uncoated but GB-NaOH treated, GB/ED-coated, and GB/NaOH/ED-coated. A fourth group was sent for plasma spraying at a company. Implantations were done at Tel Aviv University in mature New Zealand white rabbits. The implants were press-fitted into the medullary canal. The distal portion of the implant was within the metaphysis, while the proximal portion was within the diaphysis. Analyses were made at one week and 12 weeks post-implantation. Advanced XPS analysis revealed that both types of ED-HAp consisted of both OCP and HAp, the content of the former being possibly higher in the sample pretreated with NaOH. On the other hand, the PS-HAp sample consisted of a mixture of several phases, presumably OCP, DCPD, and HAp. The PS-HAp coating was found to possess higher tendency to delaminate compared to the ED-HAp. One week post-implantation, the bone apposition ratio (BAR) values were the highest for the PS-HAp and GB/NaOH/ED-HAp groups. After 12 weeks of implantation, the BAR values were higher for all coated samples compared to the uncoated implants. No significant difference was observed between the values measured in the diaphysis and those measured in the metaphysis. The NaOH alkaline treatment per se was found to enhance the osseointegration of both uncoated and ED-HAp-coated implants. Moreover, this treatment was found to increase significantly the adhesion strength of the coating and its scratch resistance.[20,23]

EXPERIMENTAL

The experimental procedures have been described in detail elsewhere.[14,15–23] In brief, electrodeposition was carried out in a standard three-electrode cell. Either a sheet made of commercially pure Ti grade 2 (10 × 10 × 5 mm) or a rod made of Ti-6Al-4V grade 5 was used as a cathode. The exposed surface area of the working electrode was either 1 cm^2 or ~0.205 cm^2 in the macro-cell and AFM liquids cell, respectively. A Pt foil and a Pt wire were used as counter electrodes (anodes) in the standard macro-cell and AFM liquids cell, respectively. A saturated calomel electrode (SCE), a commercial Ag/AgCl electrode, and a Pt wire were used as reference and quasi-reference electrodes, the latter in the EC-AFM cell only. Preliminary measurements in a macro-cell (T = 60 °C, no nitrogen purging) showed that 167 min were required for the Pt wire to reach steady state at E = 398 ± 10 mV vs. SCE.[14] Surface preparations included mechanical grinding and polishing.

The electrolyte solution used for the electrodeposition of CaP was based on calcium nitrate ($Ca(NO_3)_2$) and ammonium dihydrogen phosphate ($NH_4H_2PO_4$). The powders were dissolved in Millipore water. Two types of solutions were prepared: (i) 0.61 mM $Ca(NO_3)_2$, 0.36 mM $NH_4H_2PO_4$, pH = 6.0; and (ii) 20 mM $Ca(NO_3)_2$, 12 mM $NH_4H_2PO_4$, pH = 4.2. The bath composition and pH values were matched based on the solubility isotherm for HAp in the ternary system $Ca(OH)_2$-H_3PO_4-H_2O.[26] The pH was adjusted to its initial desired value by either HCl or NaOH additions. During the electrodeposition process itself, CO_2-free nitrogen gas (99.999% purity) was continuously purged into the electrolyte to minimize the risk of contamination of the deposits by carbonates. In addition, stirring was carried out. Constant temperature (within the range of room temperature to 95 °C) was maintained. The cathode potential was kept constant at –1.4 V vs. SCE for 2–3 h. A bi-potentionstat/galvanostat was used in the EC-AFM. Potentiodynamic experiments at a scan rate of 0.5 mV/s were conducted in a macro-cell both in electrolyte (i) and in a supporting electrolyte, where the 0.61 mM $Ca(NO_3)_2$ was replaced by 1.22 mM $NaNO_3$. Because sodium phosphate is soluble in aqueous solutions, the subtraction of currents measured in the supporting electrolyte from currents measured in the standard electrolyte provides the net current associated with nucleation and growth of HAp. Preliminary cyclic voltammetry (CV) experiments were also carried out in a macro-cell, with a standard electrolyte at 60 °C. A scan rate of 100 mV/s was found to be the fastest to still yield overlap of voltammograms.[14]

The samples were weighed before and after deposition. The structure of the deposits was analyzed by X-ray diffraction. Fourier transform infrared (FT-IR) spectroscopy was used to determine the vibration modes characteristic of the CaP coating. The morphology of the deposits after drying was imaged by scanning electron microscope (SEM). The attached energy dispersive spectroscopy was used to estimate the Ca/P ratio as well as to identify other elements present in the deposit. Metallographic cross sections were also prepared and analyzed for thickness, adhesion, and morphology. The thickness of the coating was also measured by SEM.

An electrochemical atomic force microscope (EC-AFM) was used both ex situ and in situ.[14,16] Imaging was done under contact mode. Both topography and deflection (error signal) images were acquired. The mean length and mean width of the CaP crystals were determined by direct measurement of features on the deflection image. The mean thickness, on the other hand, was determined from line scans on the topography image. In situ CV and cathodic polarization experiments were conducted at 5 mV/s while imaging the surface. This very slow scan rate allowed for correlating the acquired image with the cyclic voltammogram.

In the electrochemical quartz crystal microbalance (EQCM) experiments, a quartz crystal element (AT-cut, 6 MHz) coated with pure Ti was used as the working electrode. The upper metal electrode had a diameter d = 1.3 cm and an effective surface area A = 1.327 cm^2. The cell contained 30 mL of electrolyte (i). A potentiostatic mode was

employed, setting the cathode potential at –1.29 V vs. SCE for 40 min. Neither purging nor stirring was carried out during the experiment. The bath temperature was fixed at 65 °C. An electrode resonance stability experiment was carried out prior to the electrodeposition experiment. The complete setup (i.e., mass sensor, electrode, and electrolyte solution) was first placed inside a thermostatic bath. Twenty minutes after reaching 65 °C, the stability experiment began and the variation in frequency was monitored for nearly 40 min in the absence of applied potential. The electrodeposition experiment itself started immediately after applying potential to the cell.[15] X-ray photoelectron spectroscopy (XPS) measurements were performed in order to determine unambiguously the CaP phase that formed during the EQCM experiment, so that the number of electrons transferred in the reaction could be determined. To this aim, the Ca/P and O/Ca atomic ratios were measured and the oxygen loss spectrum was analyzed, according to the procedure suggested by Lu et al.[15,27]

An innovative post-treatment was also applied, by exposing some coated samples to low-energy electron irradiation, thus modifying the surface energy on the nanoscale.[19,21,28] However, this will not be presented in this paper.

RESULTS AND DISCUSSION

The Mechanism of Electrocrystallization

The dependence of the measured weight of coatings deposited at pH = 6.0 for 3 h on the bath temperature is shown in Fig. 1.[17] The coating weight was found to increase with increasing temperature. Plotting the data from Fig. 1 in the form of v versus $1/T$, where v is the deposition rate (in units of g/(h·m^2)) and T is the absolute temperature, the following relation was obtained:[15,16]

$$\mathrm{Ln}(v) = 14.74 - 4,785\frac{1}{T},\ R^2 = 0.9742 \qquad (1)$$

where R^2 is the determination coefficient. It should be noted that the relatively low value of R^2 results from the narrow range of temperatures (70–95 °C), based on which eq 1 was derived. This narrow temperature range was associated with the conditions under which good electrodeposits of HAp could be formed on CP-Ti from the same bath.[17] Comparing to Arrhenius equation

$$v = A^* \exp\left(-\frac{\Delta G^{\ddagger}}{RT}\right) \qquad (2)$$

the standard enthalpy of activation was estimated to be

$$\Delta H^{\ddagger} \approx 40 \pm 4 \text{ kJ/mol} \qquad (3)$$

In eq 2, A^* is a pre-exponential factor, R is the ideal gas constant, and $\Delta G^{\ddagger} = \Delta H^{\ddagger} - T\Delta S^{\ddagger}$ is Gibbs energy of activation (standard free energy of activation). Equation 2 is derived based on the transition-state theory (also known as the activated complex theory). The value of the standard enthalpy of activation given in eq 3 is similar to the values reported by other investigators for apatite

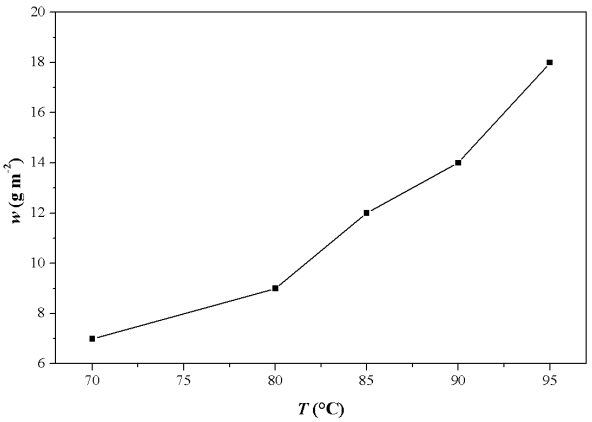

Fig. 1. The dependence of the measured weight of coatings deposited at pH = 6.0 for 3 h on the bath temperature.[17] Reprinted with permission from Crystal Growth & Design. Copyright 2008, American Chemical Society.

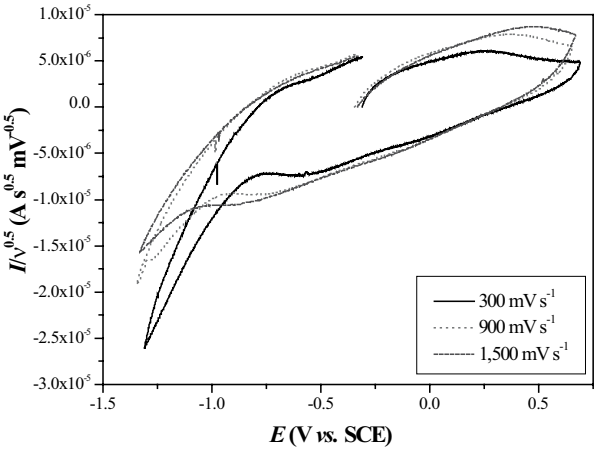

Fig. 2. Normalized cyclic voltammograms for Ti-6Al-4V in a macro-cell at 60 °C. The non-overlapping curves indicate that mass transport is not the rate-limiting step in the electrocrystallization of CaP.[14] Reprinted with permission from John Wiley & Sons.

growth,[29,30] and is within the range typical of a wide variety of mineral-solution alteration processes.[31] Furthermore, while it is too high for a bulk diffusion-controlled process, it is possible for reaction kinetics controlled by the interfacial area.[32]

Figure 2 shows three cyclic voltammograms that were constructed at different scan rates and normalized, each by the square root of its own scan rate.[14] While the normalized anodic current increases as the scan rate is increased, the normalized cathodic current decreases. Before normalization, the same voltammograms overlapped on the cathodic side. Because the normalized voltammograms do not overlap, it may be concluded that mass transport may have only a secondary role in deposition of CaP, whereas charge transfer most likely controls the process kinetically. This finding is somehow

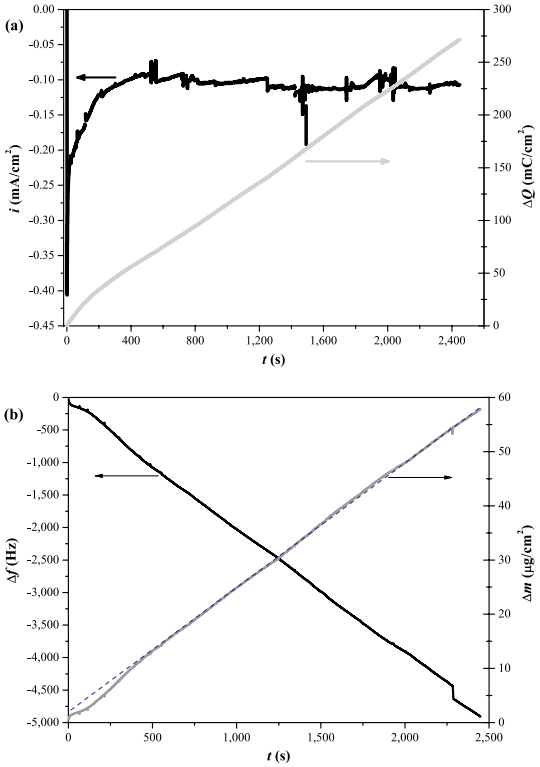

Fig. 3. (a) The potentiostatic cathodic current transient and the related time dependence of accumulated charge density during electrodeposition of CaP on an EQCM electrode. (b) The time dependence of frequency change and mass gain, the latter calculated using the Sauerbrey equation.[15] Reprinted with permission from John Wiley & Sons.

in contradiction to previous reports that focused on mass transport in nucleation and growth of HAp. However, in most cases this was an assumption rather than based on electrochemical or other direct measurements.

Figure 3a presents the potentiostatic current transient and the related time-dependence of the accumulated charge density ΔQ during an EQCM experiment. During the first 11 min, the ΔQ-versus-time curve was non-linear, and the charge values were higher than those extrapolated from the linear regime. Then, however, ΔQ increased linearly with time. Figure 3b shows the measured frequency change and the corresponding mass gain, as calculated by the Sauerbrey equation. The dashed line illustrates that, except during the first 7.3 min or so, the mass increased linearly with time. The linear dependencies of ΔQ and Δm on time indicate that a Faradaic reaction was taking place. During the first 7.3 min, the mass gain was not linear, and its values were lower than those extrapolated from the linear regime. This initial behavior may be a sign of some sort of incubation time, e.g., due to the need for the pH in vicinity of the working electrode to increase to above a certain limit. The incubation time is shorter than the time period during which ΔQ deviated from linearity. A possible explanation is that during the early 11 min, at least two different processes were monitored by the EQCM, e.g., the effect of local increase of the pH and the nucleation of a precursor with lower mass density and higher charge density. Future EQCM experiments, to be carried out with the same ion concentrations but adjusted to different pH values, are expected to show that with the increase of pH, the incubation time is shortened.[15]

Several electrochemical and chemical reactions potentially involved in electrocrystallization of CaP on Ti are listed below. Under cathodic polarization, the following electrochemical reactions may take place:[14]

$$O_2 + 2H_2O + 4e^- \rightarrow 4(OH)^-_{ads} \quad (4.1)$$

$$2H^+ + 2e^- \rightarrow H_2 \quad (4.2)$$

$$2H_2O + 2e^- \rightarrow H_2 + 2(OH)^-_{ads} \quad (4.3)$$

$$NO_3^- + H_2O + 2e^- \rightarrow NO_2^- + 2(OH)^-_{ads} \quad (4.4)$$

$$TiO_2 + 2H_2O + e^- \rightarrow Ti(OH)_3 + (OH)^-_{ads} \quad (4.5)$$

$$H_2PO_4^- + H_2O + 2e^- \rightarrow H_2PO_3^- + 2(OH)^-_{ads} \quad (4.6)$$

$$H_2PO_4^- + e^- \rightarrow HPO_4^{2-} + \frac{1}{2}H_2 \quad (4.7)$$

$$H_2PO_4^- + 2e^- \rightarrow PO_4^{3-} + H_2 \quad (4.8)$$

$$H_2PO_4^- + (OH)^-_{ads} \rightarrow PO_4^{3-} + H_2O$$

or

$$H_2PO_4^- + e^- \rightarrow PO_4^{3-} + \frac{1}{2}H_2 \quad (4.9)$$

Reactions 4.1 through 4.6 all lead to a local increase in pH within the diffusion layer. The increase in the concentration of the hydroxyl ions results in an increase in the concentration of phosphate ions, which are required for the deposition of HAp, according to reaction 4.9. Calculation of the limiting current densities i_L of these reactions showed that electrolysis of water (reaction 4.3) had by far the highest i_L value (6.4 A/cm^2). This high value can explain the absence of a limiting current density in the cyclic voltammograms. The following values were 224, 81, 56, 28, and 14 μA/cm^2 for reactions 4.4, 4.1, 4.8, 4.6, and 4.7, respectively.[14] The idea that much current is consumed during the process of electrocrystallization of CaP on electrolysis of water is supported by calculation of a very low equivalent weight (EW = 20.5 g/equiv). This value, which is based on EQCM data, means that a high number of electrons, $n \approx 24$, were transferred in the reactions that formed one mole of the product. The importance of identifying the

exact CaP phase that had been formed by electrocrystallization when calculating the value of *n* was demonstrated before.[15] It was shown that this value may change from ~7 to ~25, for DCPA and HAp, respectively.

Even when significant concentrations of phosphate ions are produced by reduction of hydrogen phosphate ions and dihydrogen phosphate ions, as in reactions 4.8 and 4.9, one should consider the fast kinetics of the phosphate ions recombination with hydrogen ions. This implies that the concentration of calcium ions in solution must be high compared to the concentration of hydrogen ions, thus statistically allowing physical precipitation of CaP in solution. The experimental conditions in the present work satisfy this requirement, with the concentrations of calcium and hydrogen cations being 0.61 mM and 1.0 μM, respectively.[14]

The electrolyte solutions in this study contained dihydrogen phosphate. Its deprotonation reaction, forming HPO_4^{2-}, serves as an important biological buffer system, which operates in the internal fluid of all cells, stabilizing the pH at around 7.21 (in mammals, pH = 6.9–7.4). Thus, the speciation curves of phosphoric acid may aid, at least to some extent, in understanding the effect of pH on the electrocrystallization of CaP. The relevant acid dissociation equilibrium constants at 37 °C are $K_{a1} = 5.861 \times 10^{-3}$, $K_{a2} = 6.839 \times 10^{-8}$, and $K_{a3} = 6.607 \times 10^{-13}$.[33,34] We have used the chemical equilibrium code ChemEQL version 3.010[35] to generate these speciation curves, as shown in Fig. 4.[16] The total analytical concentration of phosphate was defined as 0.36 mM. This figure shows the speciation of phosphoric acid at 37 °C. It is evident that once the solution is prepared, some of the $H_2PO_4^-$ ions deprotonate, forming HPO_4^{2-}. For pH values in the range of 7.2–12.0, the predominant species is HPO_4^{2-}, whereas above pH = 12.0 the triply-charged anion PO_4^{3-} becomes the most abundant species. Similar calculations can be made for the bath at $pH_0 = 4.2$. In this case, however, some of the $H_2PO_4^-$ ions immediately protonate, forming H_3PO_4. It should be emphasized that only orthophosphate salts are considered herein, because metaphosphates and pyrophosphates hydrolyze in body fluids. Thus, it is evident that the local pH in vicinity of the working electrode must first increase significantly before pronounced precipitation of HAp can take place. This conclusion is supported by the incubation period observed in the EQCM plots.

In several papers (e.g., refs 36–44), deposition of apatite bioceramics from electrolytes has been assumed to follow one or more of the following reactions: (1) electrochemical reactions, (2) acid–base reactions, and (3) physical precipitation from solution. Based on their experimental results, Eliaz and Eliyahu suggested the model shown in Fig. 5 for the formation of HAp by

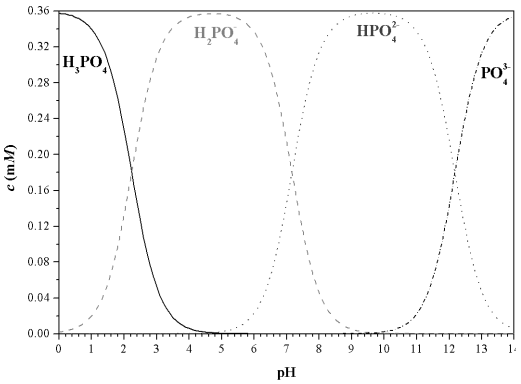

Fig. 4. The distribution of phosphate species as a function of pH at 37 °C, 0.36 mM total analytical concentration of phosphate, and free hydrogen concentration of 10^{-6} M.[16] Reprinted with permission from Crystal Growth & Design. Copyright 2008, American Chemical Society.

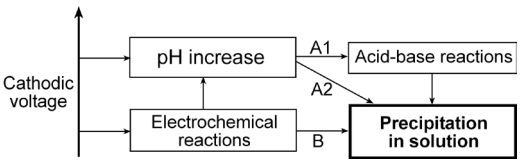

Fig. 5. The processes that allow formation of HAp in electrolytes. Following route A1, the increase in pH first facilitates chemical deprotonation reactions. In route A2, the increase in pH lowers the solubility of the apatite phase in accordance with the solubility isotherms. Following route B, the potential is cathodic enough to allow direct production of sufficient phosphate ions according to reactions 4.8 and 4.9 (the former being more dominant).[14] Reprinted with permission from John Wiley & Sons.

electrocrystallization.[14] According to this model, a sufficiently cathodic potential allows for various interplays between electrochemical reactions, chemical reactions and local pH increase. The three possible routes may all result in precipitation of HAp in solution.

Once the proper composition and pH of the electrolyte solution are established in vicinity of the cathode, the following precipitation reactions (among others) may occur:

$$5(Ca^{2+}) + 3(PO_4^{3-}) + (OH)^- \leftrightarrow HAp \qquad (5.1)$$

$$4(Ca^{2+}) + 3(PO_4^{3-}) + H^+ + 2.5H_2O \leftrightarrow OCP \qquad (5.2)$$

or

$$4(Ca^{2+}) + 3(HPO_4^{2-}) + 2.5H_2O \leftrightarrow OCP + 2H^+ \qquad (5.3)$$

Comparing between reactions 5.2 and 5.3, the latter may have higher probability to actually occur under the studied conditions because: (1) it requires HPO_4^{2-}, not PO_4^{3-}, and therefore does not need the pH to increase as much; and (2) the production of the hydrogen cations partly compensates for the production of hydroxyl ions, thus the increase of pH is slowed down.

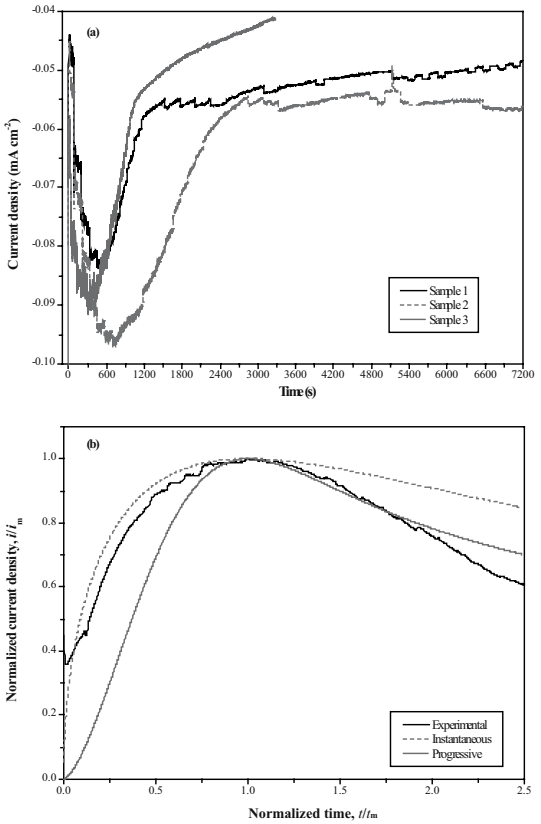

Fig. 6. Current density transients during electrocrystallization of HAp on CP-Ti. (a) Experimental data from three potentiostatic experiments at T = 80–85°C. (b) A normalized experimental transient is compared to the counterpart calculated curves for instantaneous and progressive nucleation models. A change is observed from instantaneous nucleation at shorter deposition periods to progressive nucleation at longer periods.[14] Reprinted with permission from John Wiley & Sons.

The Role of Precursors

The nucleation process on real crystalline substrates with a fixed number, N_0, of randomly distributed, equally active sites may be described by the following first-order kinetics law:[13,45,46]

$$N = N_0[1 - \exp(-At)] \quad (6)$$

where N is the number of sites converted into nuclei at time t and A is a nucleation rate constant. When A is very high, all surface sites are converted immediately into nuclei and the nucleation is said to be "instantaneous". On the other hand, when A and t are both small, the number of nuclei depends on time and the nucleation is termed "progressive".

The most important parameters determining the mode of growth of a substance on a foreign substrate are the deposit/substrate binding energy and the crystallographic misfit between them. Considering the deposition process at nearly equilibrium conditions, i.e., small supersaturation and negligible kinetic influences, a deposit may grow on a substrate by different modes, e.g., in accordance with the Frank–van der Merwe, Volmer-Weber, or Stranski–Krastanov models.[13]

Figure 6a shows the current density transients monitored during potentiostatic deposition at –1.4 V vs. SCE. The shape of these transients is similar to that drawn for theoretical transients in the presence of overlap between diffusion fields around growing nuclei.[14,47] Based on Fig. 6a it may be concluded that after approximately 12 min at 80–85 °C, the CaP deposit changed its morphology from two-dimensional (2D) to three-dimensional (3D).

Scharifker et al. derived analytical expressions for multiple nucleation phenomena followed by diffusion-controlled growth of 3D islands.[48,49] The resulting expressions for the normalized current densities allow distinguishing between instantaneous nucleation and progressive nucleation:[48,50]

$$\frac{i^2}{i_m^2} = 1.9542\frac{t_m}{t}\left[1 - \exp\left(-1.2564\frac{t}{t_m}\right)\right]^2$$

instantaneous (7.1)

$$\frac{i^2}{i_m^2} = 1.2254\frac{t_m}{t}\left[1 - \exp\left(-2.3367\frac{t^2}{t_m^2}\right)\right]^2$$

progressive (7.2)

where i_m is the maximum current density in the current density transient and t_m is the time at this maximum point. Figure 6b is a normalized representation of an experimental current density transient with t_m = 1,108 s and i_m = –88.3 μA/cm^2. For comparison, the calculated curves for instantaneous nucleation and progressive nucleation are also drawn. It is evident that while at times shorter than t_m the experimental curve fits better the instantaneous nucleation model, at times longer than t_m it fits better the progressive nucleation model. The deviation of the experimental curve from the theoretical curves may be explained in terms of both accompanying cathodic reactions in which charge is transferred, and precipitation from solution instead of direct nucleation on the solid electrode surface. The change from instantaneous nucleation to progressive nucleation may be attributed to the formation of a precursor, porosity and non-uniform electrical fields in the ceramic HAp coating, as well as from changes in the pH and composition of the solution during the experiment. It should be noted that a similar change occurs in electrodeposition of metal on metal or metal on semiconductor only when the applied

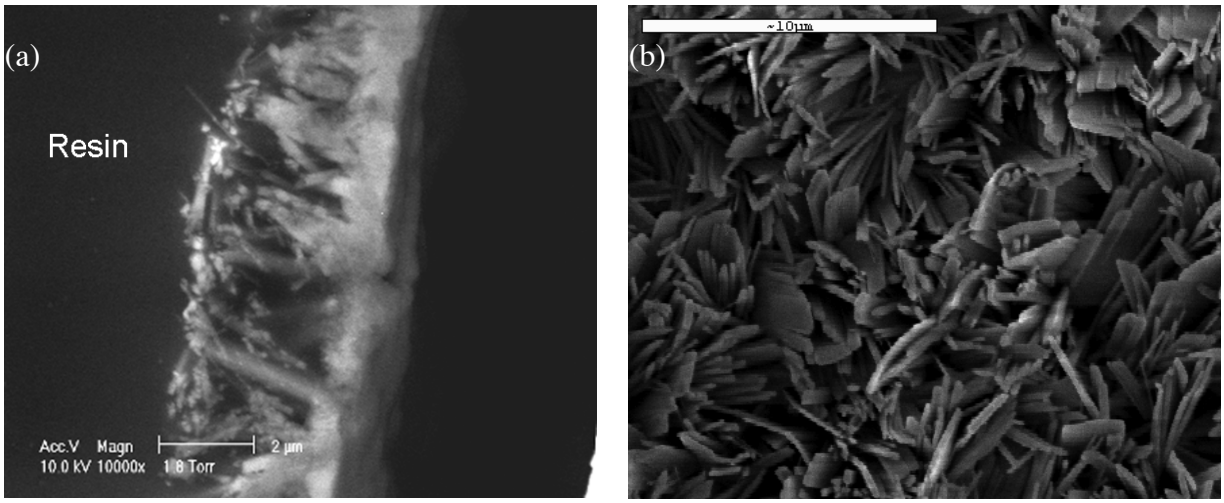

Fig. 7. (a) ESEM image of a cross section of ED-HAp coating, demonstrating two layers.[51] Reprinted with permission. Copyright 2009, Research Signpost. (b) Typical surface morphology (SEM) of HAp coating deposited at $pH_0 = 6.0$ and 80 °C for 3 h. The scale bar is 10 µm long.[16] Reprinted with permission from Crystal Growth & Design. Copyright 2008, American Chemical Society.

potential is changed, and that in these cases the timescale for instantaneous nucleation is much shorter (namely, t_m is typically within the milliseconds to seconds range) than that in the experiments reported herein. These differences further support the claim that the mechanism of electrocrystallization of HAp is basically different from conventional electrodeposition of metals.[14]

ESEM study showed (see Fig. 7a) that the deposit that had been formed on the titanium consisted of two layers: (1) a uniform, 500-nm-thick dense layer adjacent to the substrate; and (2) a thicker layer composed of crystals with varying sizes.[22,51] Figure 7b shows the typical surface morphology of an ED-HAp coating deposited at $pH_0 = 6.0$ and 80 °C for 3 h. A platelets morphology is evident, with each platelet being presumably composed of whiskers. The Ca/P ratio for this coating (EDS) was 1.65. Transmission electron microscopy also revealed that formation of nano-sized cubical crystals was followed by growth of columnar single crystals with preferred orientation.[22,51] These experimental results support the claim for occurrence of both instantaneous and progressive nucleation mechanisms, as well as for transition from 2D to 3D growth. Ex situ AFM study also demonstrated that a transition from 2D growth to 3D growth occurred sometime between 10 min and 30 min of deposition.[14] Interestingly, in the case of bone mineralization in a given species, the average crystal size is smallest at formation and increases to maturity, at which time there is a leveling of this growth process.[8]

Eliaz and Sridhar[16] observed substantially different current density transients when electrocrystallization took place in a bath initially at $pH_0 = 6.0$ versus when it occurred in a bath initially at $pH_0 = 4.2$. As mentioned before, while at pH = 6.0 only the HAp phase was observed, at $pH_0 = 4.2$ traces of OCP were observed too. When increasing the bath temperature to 90 °C, the content of OCP decreased and that of HAp increased. This behavior is in accordance with a previous observation that pH values lower than 4.4 would require high temperatures for the precipitation of stoichiometric HAp.[52] In another study, XPS analysis proved the formation of OCP on the EQCM electrode.[15]

It was Ostwald who first suggested that upon phase transformation, whether crystallization, melting, or condensation, the phase that nucleates first is not necessarily the thermodynamically most stable one, but the one with free energy that is closest to the original state.[53] This statement has become known as "Ostwald's rule". In agreement with this rule, it has been suggested that several CaP phases, such as OCP, DCPD, and ACP, may serve as precursors to the formation of HAp in vivo.[6,54,55] Moreover, it has been argued that the precipitation of CaP phases from a saturated solution is not only governed by the thermodynamic solubility product, but also by kinetic factors. Thus, the precipitated phase may undergo solution-mediated transformation to more stable phases.[56] Actually, at low pH values dicalcium phosphates as brushite become more stable,[57–59] and HAp has been proposed as a precursor of brushite.[60] It has been suggested that the transformation of OCP into HAp may proceed via: (1) a process of OCP dissolution and reprecipitation of HAp crystals, and (2) in situ hydrolysis, which is accompanied by calcium consumption from the surrounding solution and release of phosphate ions into the solution.[55] Wang et al. also found that during early-stage mineralization (≤7 d), the Ca/P ratio in

the mineralized tissue adjacent to the electrodeposited HAp coating resembled that in OCP, although DCPD or ACP could not be excluded.[22] As precipitation of OCP may occur in the presence of either HPO_4^{2-} or PO_4^{3-} (see eqs 5.2 and 5.3), whereas precipitation from solution of HAp requires a supersaturated concentration of PO_4^{3-} to be established first (see eq 5.1), it may be expected that OCP will form within a lower pH range compared to HAp. Indeed, it has been reported that in aqueous solutions at 25 °C, the pH stability ranges for OCP and HAp are 5.5–7.0 and 9.5–12.0, respectively.[5]

The very high value of pH that is required to favor the formation of PO_4^{3-} by chemical reactions, according to Fig. 4, is obviously unattainable in vivo. Therefore, the following conclusions may be drawn: (1) The formation of either OCP or HAp may not be under simple chemical equilibrium conditions. (2) The solubility product K_{sp} must be very low, allowing precipitation of CaP even at relatively low concentrations of calcium and phosphate/hydrogen phosphate ions. Indeed, pK_{sp} values of 47.08 and 58.6 have been reported for OCP and HAp at 37 °C, respectively.[61] It is well known that CaP salts are only sparingly soluble in aqueous solutions. (3) It is more likely for HAp to form via transformation of precursor phases, such as OCP, rather than directly. The author assumes that in those studies, where no precursor was observed, the reason may be either its morphological and structural similarity to HAp (in the case of OCP), conversion over time to the more stable HAp, or the use of insensitive analytical techniques for determination of the chemical composition of the coating just at the interface with the substrate. (4) The precipitation from solution of CaP may take place only within a very small volume adjacent to the surface of the substrate.

CONCLUSIONS

In this paper, the work carried out at Tel Aviv University on electrocrystallization of CaP was reviewed. The following conclusions were drawn:

1. Except for a short incubation time, the process by which the CaP is formed was found to follow a Faradaic behavior, thus demonstrating the important role that charge transfer plays. The incubation time may be related to the need for local increase of pH before precipitation from solution can take place. The high equivalent weight value of 20.5 g/equiv, and the associated remarkably high number of electrons transferred in the reaction n~24, indicate that most of the current is consumed either by electrolysis of water or by a complex set of parasitic reactions.
2. Based on the experimental data, the standard enthalpy of activation was calculated to be approximately 40 kJ/mol. This high value is typical of interfacial reactions, and indicates that diffusion in the bulk solution did not play a major role in the electrocrystallization process.
3. Electrocrystallization of HAp was shown to result from precipitation in solution, following two stages: (i) instantaneous nucleation, 2D growth, and (ii) progressive nucleation, 3D growth.
4. Calculations based on acid dissociation equilibrium constants and solubility products indicate that HAp may most likely form via transformation of precursor phases, such as OCP, rather than directly. The very low solubility product allows precipitation of CaP even at relatively low concentrations of calcium and phosphate/hydrogen phosphate ions.

Acknowledgments. The author is thankful to past and present members of the Biomaterials and Corrosion Laboratory, namely T.M. Sridhar, D. Lakstein, M. Eliyahu, S. Shmueli, W. Kopelovitch, and O. Ritman, for their dedicated work and significant contributions. The author is grateful to the Dan David, Ella Kodesh, and Pikovsky Valachi Foundations as well as to the Japanese Society for the Promotion of Science for their financial support. The collaborations with L.W. Hobbs, T. Hanawa, D. Hendel, G. Rosenman, D. Benayahu, M. Weinreb, and E.Z. Ron as well as the fruitful discussions with E. Gileadi are highly appreciated.

REFERENCES AND NOTES

(1) Eliaz, N. In *Corrosion Science and Technology: Mechanism, Mitigation and Monitoring*; Kamachi Mudali, U.; Raj, Baldev, Eds.; Narosa Publishing House: India, 2008, Chapter 12, pp 356–397.
(2) Hong, S.-B.; Eliaz, N.; Sachs, E.M.; Allen, S.M.; Latanision, R.M. *Corros. Sci.* **2001**, *43*, 1781–1791.
(3) Hong, S.-B.; Eliaz, N.; Leisk, G.G.; Sachs, E.M.; Latanision, R.M.; Allen, S.M. *J. Dent. Res.* **2001**, *80*, 860–863.
(4) Eliaz, N.; Nissan, O. *J. Biomed. Mater. Res. A* **2007**, *83*, 546–557.
(5) Dorozhkin, S.V.; Epple, M. *Angew. Chem. Int. Ed.* **2002**, *41*, 3130–3146.
(6) Johnsson, M.S.A.; Nancollas, G.H. *Crit. Rev. Oral Biol. Med.* **1992**, *3*, 61–82.
(7) de Leeuw, N.H. *Chem. Commun.* **2001**, *17*, 1646–1647.
(8) Betts, F.; Blumenthal, N.C.; Posner, A.S. *J. Cryst. Growth* **1981**, *53*, 63–73.
(9) Benezra, V.; Spector, M.; Hobbs, L.W. In *Proc. 1995 Materials Research Society Fall Meeting*; Cotell, C.M.; Meyer, A.E.; Gorbatkin, S.M.; Grobe, G.L., Eds.; MRS: PA, 1996, Vol. 414, pp 165–170.
(10) Danilchenko, S.N.; Kukharenko, O.G.; Moseke, C.; Protsenko, I.Y.; Sukhodub, L.F.; Sulkio-Cleff, B. *Cryst. Res. Technol.* **2002**, *37*, 1234–1240.

(11) Nyman, J.S.; Reyes, M.; Wang, X. *Micron* **2005**, *36*, 566–582.
(12) Prendergast, P.J. *Encyclopedia of Medical Devices and Instrumentation*; Webster, J.G., Ed.; Wiley: NY, 2006, pp 192–198.
(13) Budevski, E; Staikov, G.; Lorenz, W.J. *Electrochemical Phase Formation and Growth: An Introduction to the Initial Stages of Metal Deposition*; VCH: Weinheim, Germany, 1996, pp, 4–6, 163–165, 184–185, 280–283, 342.
(14) Eliaz, N.; Eliyahu, M. *J. Biomed. Mater. Res. A* **2007**, *80*, 621–634.
(15) Eliaz, N.; Kopelovitch, W.; Burstein, L.; Kobayashi, E.; Hanawa, T. *J. Biomed. Mater. Res. A*, in press. DOI 10.1002/jbm.a.32120
(16) Eliaz, N.; Sridhar, T.M. *Cryst. Growth Des.* **2008**, *8*, 3965–3977.
(17) Eliaz, N.; Sridhar, T.M.; Rosenberg, Yu. In *Proc. of the 10th World Conf. on Titanium*; Lütjering, G.; Albrecht, J., Eds.; Wiley-VCH: Weinheim, Germany, 2004, Vol. V, pp 3299–3306.
(18) Eliaz, N.; Sridhar, T.M.; Kamachi Mudali, U.; Raj, Baldev. *Surf. Eng.* **2005**, *21*, 238–242.
(19) Shmueli, S. M.Sc. Thesis. Tel Aviv Univ., Israel, 2007.
(20) Kopelovitch, W. M.Sc. Thesis. Tel Aviv Univ., Israel, 2008.
(21) Ritman, O. M.Sc. Thesis. Tel Aviv Univ., Israel, 2008.
(22) Wang, H.; Eliaz, N.; Xiang, Z.; Hsu, H.-P.; Spector, M.; Hobbs, L.W. *Biomaterials* **2006**, *27*, 4192–4203.
(23) Lakstein, D. *Basic Sciences Research in Medicine*; Tel Aviv Univ., Israel, 2007.
(24) Sridhar, T.M.; Eliaz, N.; Kamachi Mudali, U.; Raj, Baldev. *Corr. Rev.* **2002**, *20*, 255–293.
(25) Kamachi Mudali, U.; Sridhar, T.M.; Eliaz, N.; Raj, Baldev. *Corr. Rev.* **2003**, *21*, 231–267.
(26) Brown, P.W. *J. Am. Ceram. Soc.* **1992**, *75*, 17–22.
(27) Lu, H.B.; Campbell, C.T.; Graham, D.J.; Ratner, B.D. *Anal. Chem.* **2000**, *72*, 2886–2894.
(28) Aronov, D.; Rosenman, G.; Karlov, A.; Shashkin, A. *Appl. Phys. Lett.* **2006**, *88*, 163902–4.
(29) Ban, S. *Dental Mater. J.* **2003**, *22*, 467–474.
(30) Tanahashi, M.; Kokubo, T.; Matsuda, T. *J. Biomed. Mater. Res.* **1996**, *31*, 243–249.
(31) Lasaga, A.C. *Kinetic Theory in the Earth Sciences*; Princeton University Press: New Jersey, 1997.
(32) Laidler, K.J. *Chemical Kinetics*; McGraw-Hill: New York, 1958.
(33) Sillén, L.R.; Martell, A.E. *Stability Constants of Metal-Ion Complexes*; The Chemical Society: London, 1964, Supplement 17, pp 180–181.
(34) Koutsoukos, P.; Amjad, Z.; Tomson, M.B.; Nancollas, G.H. *J. Am. Chem. Soc.* **1980**, *102*, 1553–1557.
(35) Müller, B. *Manual of ChemEQL (Version 3.0)*; Limnological Research Center EAWAG/ETH: Kastanienbaum, Switzerland, 2004.
(36) Zhang, J.M.; Lin, C.J.; Feng, Z.D.; Tian, Z.W. *J. Electroanal. Chem.* **1998**, *452*, 235–240.
(37) Huang, L.Y.; Xu, K.W.; Lu, J. *J. Mater. Sci.: Mater. Med.* **2000**, *11*, 667–673.
(38) Kumar, M.; Dasarathy, H.; Riley, C. *J. Biomed. Mater. Res.* **1999**, *45*, 302–310.
(39) Kuo, M.C.; Yen, S.K. *Mater. Sci. Eng. C* **2002**, *20*, 153–160.
(40) Redepenning, J.; Schlessinger, T.; Burnham, S.; Lippiello, L.; Miyano, J. *J. Biomed. Mater. Res.* **1996**, *30*, 287-294.
(41) Shirkhanzadeh, M. *J. Mater. Sci.: Mater. Med.* **1998**, *9*, 67–72.
(42) Yen, S.K.; Lin, C.M. *Mater. Chem. Phys.* **2002**, *77*, 70–76.
(43) Moreno, E.C.; Varughese, K. *J. Cryst. Growth* **1981**, *53*, 20–30.
(44) Brown, W.E.; Chow, L.C. *J. Cryst. Growth* **1981**, *53*, 31–41.
(45) Fleischmann, M.; Thirsk, H.R. In *Advances in Electrochemistry and Electrochemical Engineering*; Delahay, P., Ed.; Wiley, New York, 1963, Vol. 3, p 123.
(46) Milchev, A. *Electrochim Acta* **1997**, *42*, 1533–1536.
(47) Paunovic, M.; Schlesinger, M. *Fundamentals of Electrochemical Deposition*; John Wiley & Sons: New York, 1998.
(48) Scharifker, B.; Hills, G. *Electrochim Acta* **1983**, *28*, 879–889.
(49) Scharifker, B.R.; Mostany, J.; Palomar-Pardavé, M.; González, I. *J. Electrochem. Soc.* **1999**, *146*, 1005–1012.
(50) Oskam, G.; Long, J.G.; Natarajan, A.; Searson P.C. *J. Phys. D.: Appl. Phys.* **1998**; *31*, 1927–1949.
(51) Wang, H.; Eliaz, N.; Hobbs, L.W. In *Recent Developments in Advanced Medical and Dental Materials Using Electrochemical Methodologies*; Karlinsky, R.L., Ed.; Research Signpost: Trivandrum, Kerala, India, 2009.
(52) Le Geros, R.Z. *Calcium Phosphates in Oral Biology and Medicine, Monographs in Oral Science*; Meyers, H.M., Ed.; Karger: Basel, 1991, Vol. 15, pp 19–67.
(53) Ostwald, W. *Z. Phys. Chem.* **1897**, *22*, 289–302 (in German).
(54) Brown W.E.; Eidelman, N.; Tomazic, B. *Adv. Dent. Res.* **1987**, *1*, 306–313.
(55) Suzuki, O.; Kamakura, S.; Katagiri, T. *J. Biomed. Mater. Res. B* **2006**, *77*, 201–212.
(56) Abbona, F.; Lundager Madsen, H.E.; Boistelle, R. *J. Cryst. Growth* **1986**, *74*, 581–590.
(57) Elliot, J.C. *Structure and Chemistry of the Apatites and other Calcium Orthophosphates*; Elsevier: Amsterdam, 1994.
(58) Nancollas, G.H. In *Phosphate Minerals*; Nriagu, J.O.; Moore, P.B., Eds.; Springer-Verlag: Berlin, 1984, pp 137–154.
(59) Nancollas, G.H.; Zhang, J. In *Hydroxyapatite and Related Materials*; Brown, P.W.; Constantz, B., Eds.; CRC Press: Boca Raton, FL, 1994, pp 73–82.
(60) Ferreira, A.; Oliveira, C.; Rocha, F. *J. Cryst. Growth* **2003**, *252*, 599–611.
(61) Koutsoukos, P.; Amjad, Z.; Tomson, M.B.; Nancollas, G.H. *J. Am. Chem. Soc.* **1980**, *102*, 1553–1557.